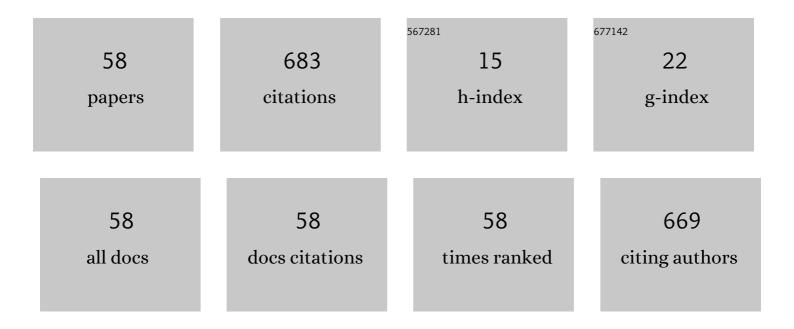
## Shuangmeng Zhai

List of Publications by Year in descending order

Source: https://exaly.com/author-pdf/241135/publications.pdf Version: 2024-02-01



#	Article	IF	CITATIONS
1	Phase transition of Mg3(PO4)2 polymorphs at high-temperature: In-situ synchrotron X-ray diffraction and Raman spectroscopic study. Spectrochimica Acta - Part A: Molecular and Biomolecular Spectroscopy, 2022, 269, 120762.	3.9	4
2	Electrical and thermal conductivity of Earth's core and its thermal evolution—A review. Acta Geochimica, 2022, 41, 665-688.	1.7	1
3	Electrical Resistivity of Fe and Feâ€3 wt%P at 5ÂGPa With Implications for the Moon's Core Conductivity and Dynamo. Journal of Geophysical Research E: Planets, 2022, 127, .	3.6	8
4	Raman spectroscopic and X-ray diffraction study of α- and β-Mg2P2O7 at various temperatures. Spectrochimica Acta - Part A: Molecular and Biomolecular Spectroscopy, 2022, 273, 121076.	3.9	3
5	Thermal expansion and compressibility of calcium scandate CaSc2O4. Journal of Alloys and Compounds, 2022, 909, 164756.	5.5	2
6	Stability of low-pressure and high-pressure CaGa2O4 polymorphs at elevated temperatures: Raman spectroscopic study. Vibrational Spectroscopy, 2022, 120, 103379.	2.2	0
7	Pressure- and temperature-dependent Raman spectra of Ca2Fe2O5 oxygen defect perovskite. Spectrochimica Acta - Part A: Molecular and Biomolecular Spectroscopy, 2022, 279, 121436.	3.9	3
8	The structure-Raman spectra relationships of Mg3(PO4)2 polymorphs: A comprehensive experimental and DFT study. Spectrochimica Acta - Part A: Molecular and Biomolecular Spectroscopy, 2021, 245, 118906.	3.9	7
9	Thermal diffusivity and thermal conductivity of alkali feldspar at 0.8–3 GPa and 300–873 K. Contributions To Mineralogy and Petrology, 2021, 176, 1.	3.1	5
10	Thermal expansion of ellinaite (β-CaCr2O4): an in-situ high temperature X-ray diffraction study. Physics and Chemistry of Minerals, 2021, 48, 1.	0.8	4
11	Raman spectra and X-ray diffraction of merrillite at various temperatures. Vibrational Spectroscopy, 2020, 106, 103005.	2.2	10
12	X-ray diffraction and Raman spectra of merrillite at high pressures. High Pressure Research, 2020, 40, 411-422.	1.2	2
13	Raman spectra of sillimanite, andalusite, and kyanite at various temperatures. Physics and Chemistry of Minerals, 2020, 47, 1.	0.8	13
14	Crystal chemistry of Eu-bearing tuite synthesized at high-pressure and high-temperature conditions. Physics and Chemistry of Minerals, 2019, 46, 157-163.	0.8	0
15	Thermal diffusivity and thermal conductivity of granitoids at 283–988 K and 0.3–1.5 GPa. American Mineralogist, 2019, 104, 1533-1545.	1.9	24
16	High-pressure in-situ X-ray diffraction and Raman spectroscopy of Ca <sub>2</sub> AlFeO <sub>5</sub> brownmillerite. High Pressure Research, 2019, 39, 92-105.	1.2	4
17	Temperature-induced phase transition of Ca2AlSiO5.5: Raman spectroscopic study. Vibrational Spectroscopy, 2019, 103, 102935.	2.2	5
18	Electrical Resistivity of Iron Phosphides at Highâ€Pressure and Highâ€Temperature Conditions With Implications for Lunar Core's Thermal Conductivity. Journal of Geophysical Research: Solid Earth, 2019, 124, 5544-5556.	3.4	15

SHUANGMENG ZHAI

#	Article	IF	CITATIONS
19	The phase diagram of the Fe-P binary system at 3â€ <sup>-</sup> GPa and implications for phosphorus in the lunar core. Geochimica Et Cosmochimica Acta, 2019, 254, 54-66.	3.9	9
20	Effect of Water on the Thermal Properties of Olivine With Implications for Lunar Internal Temperature. Journal of Geophysical Research E: Planets, 2019, 124, 3469-3481.	3.6	19
21	Pressure-dependent Raman spectra of Ba5(PO4)3Cl alforsite. Physics and Chemistry of Minerals, 2018, 45, 353-359.	0.8	2
22	Single crystal growth, crystalline structure investigation and high-pressure behavior of impurity-free siderite (FeCO3). Physics and Chemistry of Minerals, 2018, 45, 831-842.	0.8	13
23	Raman spectroscopic study of stronadelphite Sr5(PO4)3F at various temperatures. Vibrational Spectroscopy, 2018, 98, 123-127.	2.2	7
24	Effect of temperature on the Raman spectra of Ca5(PO4)3F fluorapatite. European Journal of Mineralogy, 2018, 30, 951-956.	1.3	10
25	Spin transition of ferric iron in the calciumâ€ferrite type aluminous phase. Journal of Geophysical Research: Solid Earth, 2017, 122, 5935-5944.	3.4	7
26	Raman spectroscopic study of MnAl2O4 galaxite at various pressures and temperatures. Physics and Chemistry of Minerals, 2017, 44, 163-170.	0.8	4
27	Elasticity of singleâ€crystal superhydrous phase B at simultaneous high pressureâ€ŧemperature conditions. Geophysical Research Letters, 2016, 43, 8458-8465.	4.0	18
28	Elasticity of singleâ€crystal NAL phase at high pressure: A potential source of the seismic anisotropy in the lower mantle. Journal of Geophysical Research: Solid Earth, 2016, 121, 5696-5707.	3.4	7
29	High-pressure X-ray diffraction and Raman spectroscopy of CaFe2O4-type β-CaCr2O4. Physics and Chemistry of Minerals, 2016, 43, 307-314.	0.8	11
30	Spin transition of ferric iron in the NAL phase: Implications for the seismic heterogeneities of subducted slabs in the lower mantle. Earth and Planetary Science Letters, 2016, 434, 91-100.	4.4	30
31	Equation of state of Ca2AlSiO5.5 oxygen defect perovskite. Physics and Chemistry of Minerals, 2015, 42, 327-336.	0.8	1
32	Photoluminescence properties of γ-Ca3(PO4)2:Sm3+ prepared under high-pressure and high-temperature conditions. Optical Materials, 2015, 45, 219-223.	3.6	5
33	Compressibilities of MnFe2O4 polymorphs. Physics and Chemistry of Minerals, 2015, 42, 569-577.	0.8	11
34	Pressure-dependent Raman spectra of β-Ca3(PO4)2 whitlockite. Physics and Chemistry of Minerals, 2015, 42, 303-308.	0.8	15
35	Raman spectra of stronadelphite Sr5(PO4)3F at high pressures. Physics and Chemistry of Minerals, 2015, 42, 579-585.	0.8	14
36	Trace element composition in tuite decomposed from natural apatite in high-pressure and high-temperature experiments. Science China Earth Sciences, 2014, 57, 2922-2927.	5.2	6

SHUANGMENG ZHAI

#	Article	IF	CITATIONS
37	Thermodynamic investigation on β- and γ-Ca3(PO4)2 and the phase equilibria. Physics of the Earth and Planetary Interiors, 2014, 228, 144-149.	1.9	11
38	Raman spectra of Sr3(PO4)2 and Ba3(PO4)2 orthophosphates at various temperatures. Vibrational Spectroscopy, 2014, 70, 6-11.	2.2	15
39	X-ray diffraction studies of Sr3Cr2O8 and Ba3Cr2O8 at high pressures. Solid State Communications, 2014, 200, 5-8.	1.9	2
40	Compressibility of pyrochlore-type MgZrSi2O7determined byin situX-ray diffraction in a large-volume high pressure apparatus. High Pressure Research, 2013, 33, 1-7.	1.2	6
41	A comparison of the Ca3(PO4)2 and CaSiO3 systems, with a new structure refinement of tuite synthesized at 15 GPa and 1300 ÂC. American Mineralogist, 2013, 98, 1585-1592.	1.9	22
42	P-V-T relations of Â-Ca3(PO4)2 tuite determined by in situ X-ray diffraction in a large-volume high-pressure apparatus. American Mineralogist, 2013, 98, 1811-1816.	1.9	12
43	Tuite, γ a <sub>3</sub> ( <scp>PO</scp> <sub>4</sub> ) <sub>2</sub> , formed by chlorapatite decomposition in a shock vein of the Suizhou L6 chondrite. Meteoritics and Planetary Science, 2013, 48, 1515-1523.	1.6	29
44	Synthesis and photoluminescence properties of Eu3+-doped Î <sup>3</sup> -Ca3(PO4)2. Materials Chemistry and Physics, 2012, 133, 324-327.	4.0	17
45	Phase boundary between perovskite and post-perovskite structures in MnGeO3 determined by in situ X-ray diffraction measurements using sintered diamond anvils. American Mineralogist, 2011, 96, 89-92.	1.9	10
46	Compressibility of strontium orthophosphate Sr3(PO4)2 at high pressure. Physics and Chemistry of Minerals, 2011, 38, 357-361.	0.8	20
47	Raman spectra and X-ray diffraction of tuite at various temperatures. Physics and Chemistry of Minerals, 2011, 38, 639-646.	0.8	17
48	High-pressure Raman spectroscopic studies on orthophosphates Ba3(PO4)2 and Sr3(PO4)2. Solid State Communications, 2011, 151, 276-279.	1.9	13
49	Synthesis and characterization of strontium–calcium phosphate γ-Ca3â^'xSrx(PO4)2 (0â‰æâ‰⊉). Materials Chemistry and Physics, 2010, 120, 348-350.	4.0	9
50	Highâ€pressure Raman spectra of tuite, γâ€Ca <sub>3</sub> (PO <sub>4</sub> ) <sub>2</sub> . Journal of Raman Spectroscopy, 2010, 41, 1011-1013.	2.5	26
51	X-ray diffraction study of -Ca3(PO4)2 at high pressure. Solid State Communications, 2010, 150, 443-445.	1.9	15
52	Pressure generation and investigation of the post-perovskite transformation in MgGeO3 by squeezing the Kawai-cell equipped with sintered diamond anvils. Earth and Planetary Science Letters, 2010, 293, 84-89.	4.4	43
53	Equation of state of Â-tricalcium phosphate, Â-Ca3(PO4)2, to lower mantle pressures. American Mineralogist, 2009, 94, 1388-1391.	1.9	23
54	<i>P</i> â€ <i>V</i> â€ <i>T</i> relations of wadsleyite determined by in situ Xâ€ray diffraction in a largeâ€volume highâ€pressure apparatus. Geophysical Research Letters, 2009, 36, .	4.0	27

SHUANGMENG ZHAI

#	Article	IF	CITATIONS
55	Pâ€Vâ€T relations of MgSiO <sub>3</sub> perovskite determined by in situ Xâ€ray diffraction using a largeâ€volume highâ€pressure apparatus. Geophysical Research Letters, 2009, 36, .	4.0	39
56	Si-Al distribution in high-pressure CaAl4Si2O11 phase: A 29Si and 27Al NMR study. American Mineralogist, 2009, 94, 1739-1742.	1.9	13
57	Effects of pre-heated pyrophyllite gaskets on high-pressure generation in the Kawai-type multi-anvil experiments. High Pressure Research, 2008, 28, 265-271.	1.2	7
58	Phase boundary between ilmenite and perovskite structures in MnGeO3 determined by in situ X-ray diffraction measurements. Physics and Chemistry of Minerals, 2007, 34, 269-273.	0.8	8